



HAL
open science

Diverse response of surface ozone to COVID-19 lockdown in China

Yiming Liu, Tao Wang, Trissevgeni Stavrakou, Nellie Elguindi, Thierno Doumbia, Claire Granier, Idir Bouarar, Benjamin Gaubert, Guy Brasseur

► **To cite this version:**

Yiming Liu, Tao Wang, Trissevgeni Stavrakou, Nellie Elguindi, Thierno Doumbia, et al.. Diverse response of surface ozone to COVID-19 lockdown in China. *Science of the Total Environment*, 2021, 789, pp.147739. 10.1016/j.scitotenv.2021.147739 . hal-03362718

HAL Id: hal-03362718

<https://hal.science/hal-03362718>

Submitted on 2 Oct 2021

HAL is a multi-disciplinary open access archive for the deposit and dissemination of scientific research documents, whether they are published or not. The documents may come from teaching and research institutions in France or abroad, or from public or private research centers.

L'archive ouverte pluridisciplinaire **HAL**, est destinée au dépôt et à la diffusion de documents scientifiques de niveau recherche, publiés ou non, émanant des établissements d'enseignement et de recherche français ou étrangers, des laboratoires publics ou privés.

Diverse response of surface ozone to COVID-19 lockdown in China

Yiming Liu^{a,*#}, Tao Wang^{a,*}, Trissevgeni Stavrakou^b, Nellie Elguindi^c, Thierno Doumbia^c, Claire Granier^{c,d}, Idir Bouarar^e, Benjamin Gaubert^f, Guy P. Brasseur^{a,e,f}

^aDepartment of Civil and Environmental Engineering, The Hong Kong Polytechnic University, Hong Kong, China;

^bRoyal Belgian Institute for Space Aeronomy, Brussels, Belgium;

^cLaboratoire d'Aérodologie, Toulouse, France;

^dNOAA Chemical Sciences Laboratory and CIRES/University of Colorado, Boulder, CO, USA;

^eEnvironmental Modeling Group, Max Planck Institute for Meteorology, Hamburg, Germany;

^fAtmospheric Chemistry Observations and Modeling Laboratory, National Center for Atmospheric Research, Boulder, CO, USA;

*Correspondence to: Tao Wang (cetwang@polyu.edu.hk) and Yiming Liu (liuym88@mail.sysu.edu.cn)

#Now in School of Atmospheric Science, Sun Yat-sen University, Guangzhou, China

Abstract: Ozone (O₃) is a key oxidant and pollutant in the lower atmosphere. Significant increases in surface O₃ have been reported in many cities during the COVID-19 lockdown. Here we conduct comprehensive observation and modeling analyses of surface O₃ across China for periods before and during the lockdown. We find that daytime O₃ decreased in the subtropical south, in contrast to increases in most other regions. Meteorological changes and emission reductions both contributed to the O₃ changes, with a larger impact from the former especially in central China. The plunge in nitrogen oxide (NO_x) emission contributed to O₃ increases in populated regions, whereas the reduction in volatile organic compounds (VOC) contributed to O₃ decreases across the country. Due to a decreasing level of NO_x saturation from north to south, the emission reduction in NO_x (46%) and VOC (32%) contributed to net O₃ increases in north China; the opposite effects of NO_x decrease (49%) and VOC decrease (24%) balanced out in central China, whereas the comparable decreases (45-55%) in the two precursors contributed to net O₃ declines in south China. Our study highlights the complex dependence of O₃ on its precursors and the importance of meteorology in the short-term O₃ variability.

Keywords: Surface ozone, meteorological condition, emission reduction, COVID-19

26 **1 Introduction**

27 The outbreak of coronavirus disease 2019 (COVID-19) has severely threatened public health worldwide, leading to millions
28 of deaths(WHO, 2020). China, where the first case of COVID-19 was reported in the city of Wuhan, imposed country-wide
29 measures from 23 January to 13 February 2020 to prevent the spread of the disease, including social distancing, teleworking,
30 and closure of non-essential businesses (Chinazzi et al., 2020; Li et al., 2020). These restrictions drastically reduced
31 anthropogenic activities, resulting in a sharp decrease in emissions of air pollutants (Dombia et al., 2020; Huang et al., 2020;
32 Wang et al., 2020a).

33 The huge and large-scale emission reductions during the COVID-19 lockdown can be treated as a natural outdoor experiment
34 to improve our understanding of the air pollutant's response to emission control. According to satellite and surface observations,
35 compared with the period before the lockdown, nitrogen dioxide (NO₂) concentrations decreased by over 50% in China during
36 the lockdown period(Bauwens et al., 2020; Liu et al., 2020; Shi and Brasseur, 2020; Zhang et al., 2020). The concentrations
37 of other pollutants, including SO₂, particulate matter with an aerodynamic diameter less than 2.5 μm (PM_{2.5}), particulate matter
38 with an aerodynamic diameter less than 10 μm (PM₁₀), and carbon monoxide (CO), also declined in a large area of
39 China(Miyazaki et al., 2020; Wang et al., 2020b). However, surface ozone (O₃) concentrations in northern and central China
40 increased by over 100%(Lian et al., 2020; Shi and Brasseur, 2020). Similar O₃ increases have been reported in southern Europe,
41 India, and Brazil despite the large decrease in other pollutants(Sharma et al., 2020; Sicard et al., 2020; Siciliano et al., 2020).
42 However, the underlying factors driving the O₃ changes during the city lockdowns remain unclear.

43 Surface O₃ is produced by photochemical reactions of ozone precursors, NO_x, volatile organic compounds (VOCs), and carbon
44 monoxide (CO) and can also be transported from higher levels of the atmosphere and from outside regions (Akimoto et al.,
45 2015; Liu and Wang, 2020a; Roelofs and Lelieveld, 1997). It is well known that O₃ has a non-linear dependence on its
46 precursors and that NO_x can either decrease or increase O₃ depending on the relative abundance of NO_x to VOCs (Atkinson,
47 2000; Wang et al., 2017a). In general, the O₃ production in urban areas with high NO_x/VOCs ratios is VOCs limited, and
48 reducing NO_x emissions can increase O₃ due to decreased titration of O₃ and radicals. In addition to the two precursors,

49 particulate matters can influence ozone by altering the solar irradiance and chemical reactions on aerosol surfaces (Li et al.,
50 2019b; Liu and Wang, 2020b; Stadtler et al., 2018). Meteorological factors affect surface ozone by changing transport pattern,
51 wet and dry depositions, chemical reaction rates, and natural emissions (Liu and Wang, 2020a; Lu et al., 2019).

52 The responses of ozone (and other air pollutants) to short-term emission reductions have been previously studied for a number
53 of public and political events in China, such as the Beijing Summer Olympic Games (August 2008), the Asia-Pacific Economic
54 Cooperation (APEC) meeting in Beijing (November 2014), and the G20 summit in Hangzhou (September 2016). During these
55 events, various emission-reducing measures were implemented in the cities concerned and their surrounding areas. Whereas
56 atmospheric concentrations of primary air pollutants (NO_x , CO, primary PM, and SO_2) in the concerned cities generally
57 decreased in response to the temporary control measures, the O_3 concentrations showed mixed responses. O_3 decreased after
58 emission reductions for some events (Huang et al., 2017; Wang et al., 2017b) but increased in others (Wang et al., 2010; Wang
59 et al., 2015; Wu et al., 2019). The different O_3 responses have been qualitatively attributed to differences in the meteorological
60 conditions (including regional transport of air masses) and to different control measures implemented by the local governments.

61 Compared with the previously studied situations, the COVID-19 lockdown is unique in that emissions decreased across the
62 whole country (and later worldwide) as opposed to a specific city or region, and the decreases were also much more drastic
63 than those due to transportation restrictions alone. Moreover, the COVID-19 lockdown took place in winter, whereas the
64 previous interventions occurred in summer and autumn, when meteorology and atmospheric chemistry are different from
65 winter. The present study analyzes surface O_3 data across China before and during the COVID-19 lockdown. We find that O_3
66 decreased in southern China while increasing in most other regions during the lockdown. Using a regional chemistry transport
67 model, we isolate the impacts of meteorological changes and anthropogenic emission reductions on O_3 . Our results highlight
68 the importance of meteorological influences on the short-term O_3 changes and the diverse response of O_3 to the emission
69 reductions of its precursors in different climate and emission-mix regions.

70 **2 Materials and Methods**

71 **2.1 Surface measurement data**

72 We obtained the observed concentrations of surface O₃ and other pollutants (PM_{2.5}, PM₁₀, SO₂, CO, NO₂) at 1643 stations from
73 the China National Environmental Monitoring Center (<http://106.37.208.233:20035/>). Data quality control was conducted for
74 the measurement data in accordance with previous studies(Lu et al., 2018; Song et al., 2017). Fig. 1 shows the locations of
75 these environmental monitoring sites.

76 The country-wide measures to control the spread of COVID-19 were implemented starting from 23 January 2020 (the exact
77 date varies for different cities), just before the Chinese New Year. All enterprises remained closed until no earlier than 13
78 February, except those required for essential public services, epidemic prevention and control, and residential life needs. We
79 focused on the period during the COVID-19 lockdown from 23 January to 12 February 2020 (hereafter referred to as the CLD
80 period), 3 weeks in total. We derived the changes in O₃ and other pollutants by comparing the CLD period with the 3 weeks
81 before the COVID-19 outbreak, from 2 to 22 January 2020 (hereafter referred to as the pre-CLD period). We focused on three
82 typical regions in China (Fig. 1): north China (NC, 35-41.5°N, 113-119°E, including Beijing, Tianjin, Hebei, and western
83 Shandong), central China (CC, 28.8-33°N, 108-117°E, including Hubei province, where Wuhan is situated, and the surrounding
84 regions), and south China (SC, 21.5-24°N, 111-116°E, including the Pearl River Delta and the surrounding regions). The NC
85 region is situated in the North China Plain, which is known to suffer from severe haze in winter; CC was the original epicenter
86 of the COVID-19 outbreak in China and is an important economic hub for the central regions of China; the Pearl River Delta,
87 where the megacities of Guangzhou and Shenzhen are situated, is the most developed region in southern China.

88 **2.2 Numerical modeling**

89 The CMAQ model (Community Multiscale Air Quality model, v5.2.1) was applied to simulate the O₃ mixing ratios over China
90 from 2 January to 12 February 2020. The WRF model (Weather Research and Forecasting model, v3.5.1) was driven by the
91 dataset of the National Center for Environmental Prediction (NCEP) FNL Operational Model Global Tropospheric Analyses
92 with a horizontal resolution of 1° × 1° and provided meteorological inputs for the CMAQ model. The CMAQ target domain
93 covered the continental China at a horizontal resolution of 36 km × 36 km. SAPRC07TIC (Carter, 2010; Hutzell et al., 2012)
94 and AERO6i (Murphy et al., 2017; Pye et al., 2017) were adopted as the gas-phase chemical mechanism and aerosol

95 mechanism, respectively. The CMAQ model has been improved with updated heterogeneous reactions to better predict the O₃
96 concentration; details can be found in Liu and Wang (2020a). Although the WRF-CMAQ model was run in offline mode, the
97 CMAQ model employs an in-line method that uses the concentrations of particles and O₃ predicted within a simulation to
98 calculate the solar radiation and photolysis rates (Binkowski et al., 2007). As a result, the effect of aerosol on O₃ concentrations
99 via changing the photolysis rates were also considered in the simulation. The chemical boundary conditions were provided by
100 the results of Whole Atmosphere Community Climate Model (WACCM, <https://www.acom.ucar.edu/waccm/download>). The
101 anthropogenic emissions in China were obtained from the Multi-resolution Emission Inventory for China (MEIC) in 2017
102 (<http://www.meicmodel.org>) with scaling factors to the year 2020 (Table S1, see text in Supplementary Information), which
103 were estimated based on the Three-Year Action Plan (2018–2020) issued by the government and the changes in the multi-
104 pollutant emissions of different sectors in recent years (Zheng et al., 2018). The emission adjustments during the lockdown
105 period are based on recent publications (see text in Supplementary Information). Emissions from the other countries were
106 derived from the MIX emission inventory (Li et al., 2017). International shipping emissions were taken from the Hemispheric
107 Transport Atmospheric Pollution (HTAP) emission version 2.2 dataset for 2010 (Janssens-Maenhout et al., 2015). Biogenic
108 emissions were calculated by the Model of Emissions of Gas and Aerosols from Nature (MEGAN) version 2.1 (Guenther et al.,
109 2012) with meteorological inputs from the WRF model.

110 Two experiments were conducted to investigate the impacts of meteorological changes and emission reductions on O₃ during
111 the CLD period. The first (baseline) used the same anthropogenic emissions for the pre-CLD and CLD periods, and the second
112 (Reduction case) used emission reductions of 70%, 40% and 30% for transportation, industry and power generation,
113 respectively, and a 10% increase of residential emission during the CLD period. These emission reductions for the whole
114 country were estimated according to the previous literature (Dombia et al., 2020; Huang et al., 2020; Wang et al., 2020a).
115 Comparing these two model simulations, the O₃ changes during the CLD period relative to the pre-CLD period for the
116 Reduction Case were considered to be entirely due to the meteorological changes and emission reductions. The impacts of the
117 meteorological changes (including the changes in chemical boundary conditions) were quantified by subtracting the O₃ mixing
118 ratios of the pre-CLD period from those of the CLD period for the baseline experiment, while the impacts of emission reduction

119 were estimated by comparing the O₃ mixing ratio during the CLD period between the Reduction Case and the baseline
120 experiment. Furthermore, we individually reduced the emissions of nitrogen oxide (NO_x), VOCs, CO, PM (particulate matter,
121 including PM₁₀, PM_{2.5}, black carbon, and organic carbon), and SO₂ during the CLD period to elucidate the response of O₃ to
122 each pollutant reduction.

123 The performance of the CMAQ model in simulating the O₃, NO₂, PM_{2.5}, SO₂, and CO concentrations for the Reduction Case
124 was evaluated (Fig. S1 and Table S2), showing reasonable agreements with the respective surface observations. Details of the
125 emission estimation and the model evaluation are presented in Supplementary Information.

126 **3 Results**

127 **3.1 Observed O₃ changes in different parts of China**

128 Figures 2 and 3 present the changes in observed concentrations of O₃ and other pollutants during the CLD period compared
129 with pre-CLD. The concentrations of most pollutants (SO₂, CO, PM_{2.5}, PM₁₀) that partially or fully originated from the direct
130 emissions declined in China during the lockdown. NO₂, a precursor of O₃, decreased by about 50% across the entire continental
131 China, and by similar amounts in all regions (Fig. 3b). However, the O₃ mixing ratio exhibited varying changes in different
132 regions (Fig. 2a). In NC and CC, the daily average O₃ increased significantly, by 112% and 73%, respectively (Fig. 2b); in
133 contrast, it remained almost unchanged in SC. The O₃ changes also varied between daytime (8:00-20:00 LST) and nighttime
134 (20:00-8:00 LST). During daytime, the O₃ increase in most parts of China was smaller than the daily average (Fig. 2c), 92%
135 and 71% in the NC and CC regions (Fig. 2d). In the SC region, most stations displayed a decrease in O₃ during daytime,
136 leading to a regional average O₃ drop of 14%. During nighttime, the O₃ mixing ratio increased significantly across China (Fig.
137 2e), by 154%, 77%, and 18% in NC, CC, and SC, respectively (Fig. 2f). These results reveal the diverse response of O₃ during
138 the lockdown in different regions, especially for the daytime. The changes in the O_x (NO₂+O₃) concentration (Fig. 3a), which
139 takes into account the NO titration, also varied in different regions. The daytime average O_x levels increased by 4% in NC and
140 by 11% in CC, and decreased by 29% in SC. These results suggest that the NO titration effect was not the only cause of the O₃

141 increase in northern and central China, as O_x would have decreased with sharply reduced NO_x emissions.

142 **3.2 Contribution of meteorological changes and emission reductions to O_3**

143 Ground-level O_3 is influenced by both chemical reactions of O_3 precursors and meteorology. In this study, we used the WRF-
144 CMAQ model to separate the impacts of meteorological changes and emission reductions on the changes in O_3 across China
145 (Fig. S2), which reveals significant contributions of both meteorology (over most of continental China) and emissions (mainly
146 in populated areas of eastern China). Fig. 4 shows the more detailed results for the NC, CC, and SC regions for both daytime
147 and nighttime and Fig. S3 presents the meteorological impact and emission impact in terms of percent change. The observed
148 O_3 changes in these regions were reasonably captured by the simulations. For the daytime average, the O_3 increase in NC was
149 attributed to the comparable contributions from both meteorological changes (58%) and emission reductions (42%) (Fig. 4a).
150 In CC (Fig. 4b), the meteorological change (98%) was the primary cause of the O_3 increase, whereas the contribution of
151 emission reduction was much lower (2%). In SC (Fig. 4c), the meteorological changes (73%) and emission reductions (27%)
152 both contributed to the O_3 decrease. During nighttime, the emission reduction increased O_3 in all three regions (including SC),
153 and its impact was stronger; the effect of meteorological changes weakened at night (Fig. S3).

154 **3.3 Impacts of meteorological changes on O_3**

155 The impacts of meteorological changes on O_3 for the NC, CC, and SC regions can be explained by the changes in the weather
156 pattern and specific meteorological factors. In winter, continental China is generally controlled by a cold high-pressure system
157 (Fig. 5). During our study period, the center of this high-pressure system was located in northern China, moving southward
158 from the pre-CLD to the CLD period, with weakening strength. The high-pressure system therefore became increasingly
159 dominant in southern China, and the strengthened southward winds brought colder air masses from the north (Fig. 6c), which
160 decreased the temperature locally (Fig. 6a). In contrast, in central and northern China, the winds shifted to a more northward
161 direction, transporting warmer air masses from the south (Fig. 6c), which increased the temperature (Fig. 6a). During daytime,
162 the decrease (increase) in temperature in the SC region (CC and NC regions) weakened (enhanced) the surface O_3 chemical

163 production. Biogenic emission is an important source of VOCs and thereby contributes to O₃ formation in China (Wu et al.,
164 2020). The temperature changes led to an increase (decrease) of biogenic emissions in the CC (SC) region (Fig. S4). Thus, the
165 temperature changes increased (decreased) O₃ in the CC (SC) region by influencing chemical reaction rates directly (Fu et al.,
166 2015; Steiner et al., 2010) and altering biogenic emissions indirectly (Im et al., 2011; Liu and Wang, 2020a).

167 The changes in the weather pattern also resulted in less clouds and precipitation in northern and central China, but more clouds
168 and precipitation in southern China (Fig. 6e and f). Clouds can reduce the amount of solar radiation reaching the surface and
169 thus the chemical production of O₃(Lelieveld and Crutzen, 1990), while precipitation can also reduce O₃ through the
170 scavenging of its precursors(Seinfeld and Pandis, 2006; Shan et al., 2008). The cloud and precipitation patterns therefore
171 contributed to O₃ increases in CC and NC and decreases in SC. Furthermore, in NC and CC, the significant increase in the
172 planetary boundary layer height during the lockdown (Fig. 6d) might promote the transport of O₃ from the upper air to the
173 surface, contributing to the O₃ increase in these regions (He et al., 2017; Sun et al., 2009). The increase (decrease) in specific
174 humidity in NC and CC (SC) might also have contributed to the decrease (increase) in O₃ mixing ratios in those regions (Li et
175 al., 2019c; Ma et al., 2019) (Fig. 6b). During nighttime, the changes in meteorological factors were similar to those in daytime
176 (Fig. S5) but exerted smaller impacts on O₃ changes due to the decreasing effects of temperature and cloud cover (negligible
177 biogenic emissions and solar radiation).

178 3.4 Response of O₃ to emission reductions

179 We further investigated the impact of multi-pollutant reductions on the O₃ changes. Because transportation and industrial
180 activities were reduced significantly during the lockdown and they are the major sources of NO_x (>80%) and VOCs (>60%)
181 (Fig. 7), the estimated reductions of NO_x and VOC emissions were more significant than those for CO, particulate matter (PM),
182 and SO₂ (Fig. 8a, c, e). The NO_x emission reductions were 46%, 49%, and 55% in the NC, CC, and SC regions, respectively,
183 while the respective reductions for VOC emissions were 32%, 24%, and 45%. The relationship between O₃ and the emissions
184 of its precursors is non-linear. We used the ratio of production rates between H₂O₂ and HNO₃ (P_{H₂O₂}/P_{HNO₃}) (Gaubert et al.,
185 2021; Tonnesen and Dennis, 2000) to identify the O₃ formation regime in China for the periods before and during the lockdown

186 (Fig. 9). $P_{\text{H}_2\text{O}_2}/P_{\text{HNO}_3} < 0.06$ is VOC-limited region; $P_{\text{H}_2\text{O}_2}/P_{\text{HNO}_3} \geq 0.2$ is NO_x -limited region, and $0.06 \leq P_{\text{H}_2\text{O}_2}/P_{\text{HNO}_3} < 0.2$ is
187 the transition zone. For the pre-CLD period, during daytime, the VOC-limited (or NO_x -saturated) regions included North
188 China Plain and other urban areas, while NO_x -limited regions located in southern China and other rural areas (Fig. 9a). During
189 nighttime, most regions are VOC-limited (Fig. 9c).

190 The O_3 formation regime determines the response of O_3 to the NO_x reduction during the CLD period. During daytime, NO_x
191 reduction increased O_3 in NO_x -saturated regions, but decreased it in NO_x -limited regions (Fig. 10b). We also found that
192 although the daytime O_3 formation regime in most regions shifted from the VOC-limited regime to the NO_x -limited regime
193 after the emission reductions during the CLD period, the daytime O_3 formation in the North China Plain was still controlled
194 by the VOC level (Fig. 9b), which suggests that the NO_x level is still high in this region. During nighttime, the reduction of
195 NO_x emission contributed increased O_3 due to the NO titration effect in a large areas (Fig. 10c). The reduction of VOC emission
196 decreased O_3 across China (Fig. 10d-f). As an O_3 precursor, the reduction of CO emission also contributed to a small decrease
197 in the O_3 mixing ratio (Fig. 10g-i); in contrast, the PM and SO_2 emissions reductions increased O_3 (Fig. 10j-o) through the
198 weakening of aerosol effects (Li et al., 2019a; Liu and Wang, 2020b), but their impacts were much smaller and were
199 insignificant (< 1 ppbv) due to the smaller reductions, compared with NO_x and VOCs.

200 The response of O_3 to the emission reductions in different regions depended on the levels of NO_x and VOC reductions. For the
201 daytime average, in the NO_x -saturated NC region, the O_3 increase by the NO_x reduction counteracted the O_3 decrease by the
202 VOC emission reduction, leading to the decrease in increased O_3 production rates (Fig. 11) and a substantial net O_3 increase
203 (Fig. 8b). In CC, the contributions of the NO_x and VOC reductions were comparable in magnitude, and their opposing impacts
204 resulted in only a slight change in O_3 (Fig. 8d). In the NO_x -limited SC region, the impact of the NO_x reduction on O_3 was
205 smaller than that of the reduction of VOCs, leading to the decrease in O_3 production rates (Fig. 11), and a net decrease in O_3
206 (Fig. 8f). During nighttime, the effect of the VOC reduction was weakened due to the lower rate of degradation of VOCs by
207 radicals compared with daytime, and the O_3 level increased in all three regions due to decreases in the NO titration effect (Fig.
208 11). The impacts of emission reductions on whole-day average O_3 were similar to those during daytime.

209 The above modeling results show that the contribution of NO_x reductions (by 46%–55%) to the rise of O_3 decreased from NC

210 to CC and to SC, reflecting the decreasing level of NO_x saturation from north to south. In contrast, the impact of the estimated
211 VOC reduction on O₃ increased from north to south, which can in part be attributed to the regional variation of VOC reductions.
212 In the SC region, transportation and industry are the predominant sources of VOCs (97%, compared with 85% and 60% in NC
213 and CC, respectively) (Fig. 7). During the CLD period, the reduction of VOC emission in SC (45%) was significant and
214 comparable with the NO_x reduction (55%). In contrast, the VOC reductions in the NC (32%) and CC (24%) regions were much
215 lower (Fig. 8a, c) and could not offset the impact of NO_x reduction on O₃. The residential sector (mainly household coal
216 burning) is an important source of VOC emission in the NC and CC regions, whereas its contribution is smaller in SC. The
217 residential emissions increased during the CLD period because many migrant workers came back for the Chinese New Year
218 holiday and were stranded there due to the lockdown (Wang et al., 2020a; Wang et al., 2020b).

219 **4. Conclusion**

220 The first country-wide lockdown during the COVID-19 outbreak in China drastically reduced transportation and industrial
221 activities, leading to sharp declines in air pollutant emissions from these sectors. Surface O₃ in urban areas of China responded
222 differently in the northern (increase) and southern regions (decrease) compared to the three-week period before the lockdown,
223 which can be explained by changes in meteorology and differences in the O₃ chemistry regimes and the magnitudes of
224 precursor reductions in these regions. The model simulated contributions of meteorology to daytime O₃ changes were larger
225 or comparable to most regions. The extent of VOC reduction, which suppressed O₃ formation, was insufficient to offset the
226 large NO titration effect during daytime in northern China, and that larger reductions of VOCs (e.g., from residential sectors)
227 would have been needed to reduce the O₃ concentration in the northern and central China. The rising O₃ concentration in
228 northern China during the COVID-19 lockdown and in recent winters should receive greater attention because O₃ boosts the
229 atmospheric oxidative capacity and therefore production of secondary aerosols (Fu et al., 2020; Huang et al., 2020; Zhu et al.,
230 2020), which are important components of winter haze in northern China. Our findings in China are relevant to untangling the
231 underlying factors driving the O₃ changes in other parts of the world during their COVID-19 lockdowns.

232 **Data availability**

233 The codes and data used in this study are available upon request from Yiming Liu (liuym88@mail.sysu.edu.cn) and Tao
234 Wang (cetwang@polyu.edu.hk).

235 **Acknowledgements**

236 This work was supported by the Hong Kong Research Grants Council (T24-504/17-N and A-PolyU502/16) and the
237 National Natural Science Foundation of China (91844301). We would like to thank Prof. Qiang Zhang from Tsinghua
238 University for providing the emission inventory.

239 **Author contributions**

240 T.W. initiated the research. Y.M.L. and T.W. designed the research framework. C.G., and T.D. estimated the emission
241 changes. Y.M.L. performed model simulations and drew the figures. T.W. and Y.M.L. analyzed the results. T.W. and
242 Y.M.L. wrote the paper with the contributions from all the authors.

243 **Competing interests**

244 The authors declare that they have no conflict of interest.

245 **Materials & Correspondence**

246 Correspondence and requests for materials should be addressed to T.W. or Y.M.L.

247 **Additional information**

248 Supplementary information is available for this paper.

249 **Reference**

250 Akimoto, H., Mori, Y., Sasaki, K., Nakanishi, H., Ohizumi, T., Itano, Y., 2015. Analysis of monitoring data of ground-level
251 ozone in Japan for long-term trend during 1990-2010: Causes of temporal and spatial variation. *Atmos. Environ.* 102,
252 302-310.

253 Atkinson, R., 2000. Atmospheric chemistry of VOCs and NO_x. *Atmos. Environ.* 34, 2063-2101.

254 Bauwens, M., Compernelle, S., Stavrakou, T., Müller, J.-F., van Gent, J., Eskes, H., Levelt, P.F., van der A, R., Veefkind, J.P.,
255 Vlietinck, J., Yu, H., Zehner, C., 2020. Impact of Coronavirus Outbreak on NO₂ Pollution Assessed Using TROPOMI and
256 OMI Observations. *Geophys Res Lett.* 47, e2020GL087978.

257 Binkowski, F.S., Arunachalam, S., Adelman, Z., Pinto, J.P., 2007. Examining Photolysis Rates with a Prototype Online
258 Photolysis Module in CMAQ. *J. Appl. Meteorol. Climatol.* 46, 1252-1256.

259 Carter, W.P.L., 2010. Development of the SAPRC-07 chemical mechanism. *Atmos. Environ.* 44, 5324-5335.

260 Chinazzi, M., Davis, J.T., Ajelli, M., Gioannini, C., Litvinova, M., Merler, S., Pastore y Piontti, A., Mu, K., Rossi, L., Sun, K.,
261 Viboud, C., Xiong, X., Yu, H., Halloran, M.E., Longini, I.M., Vespignani, A., 2020. The effect of travel restrictions on the
262 spread of the 2019 novel coronavirus (COVID-19) outbreak. *Science.* 368, 395-400.

263 Doumbia, T., Granier, C., Elguindi, N., Bouarar, I., Darras, S., Brasseur, G., Gaubert, B., Liu, Y.M., Shi, X.Q., Stavrakou, J.,
264 Tilmes, S., Wang, T., 2020. Changes in global air pollutant emissions during the Covid-19 pandemic: a dataset for
265 atmospheric chemistry modeling. submitted to *Earth. Sys. Sci. Data.*

266 Fu, T.M., Zheng, Y.Q., Paulot, F., Mao, J.Q., Yantosca, R.M., 2015. Positive but variable sensitivity of August surface ozone
267 to large-scale warming in the southeast United States. *Nat Clim Change.* 5, 454-458.

268 Fu, X., Wang, T., Gao, J., Wang, P., Liu, Y., Wang, S., Zhao, B., Xue, L., 2020. Persistent Heavy Winter Nitrate Pollution
269 Driven by Increased Photochemical Oxidants in Northern China. *Environ Sci Technol.* 54, 3881-3889.

270 Gaubert, B., Bouarar, I., Doumbia, T., Liu, Y., Stavrakou, T., Deroubaix, A., Darras, S., Elguindi, N., Granier, C., Lacey, F.,
271 Müller, J.-F., Shi, X., Tilmes, S., Wang, T., Brasseur, G.P., 2021. Global Changes in Secondary Atmospheric Pollutants
272 During the 2020 COVID-19 Pandemic. *Journal of Geophysical Research: Atmospheres.* 126, e2020JD034213.

273 Guenther, A.B., Jiang, X., Heald, C.L., Sakulyanontvittaya, T., Duhl, T., Emmons, L.K., Wang, X., 2012. The Model of

274 Emissions of Gases and Aerosols from Nature version 2.1 (MEGAN2.1): an extended and updated framework for
275 modeling biogenic emissions. *Geosci Model Dev.* 5, 1471-1492.

276 He, J., Gong, S., Yu, Y., Yu, L., Wu, L., Mao, H., Song, C., Zhao, S., Liu, H., Li, X., Li, R., 2017. Air pollution characteristics
277 and their relation to meteorological conditions during 2014–2015 in major Chinese cities. *Environ. Pollut.* 223, 484-496.

278 Huang, Q., Wang, T., Chen, P., Huang, X., Zhu, J., Zhuang, B., 2017. Impacts of emission reduction and meteorological
279 conditions on air quality improvement during the 2014 Youth Olympic Games in Nanjing, China. *Atmos. Chem. Phys.*
280 17, 13457-13471.

281 Huang, X., Ding, A., Gao, J., Zheng, B., Zhou, D., Qi, X., Tang, R., Wang, J., Ren, C., Nie, W., Chi, X., Xu, Z., Chen, L., Li,
282 Y., Che, F., Pang, N., Wang, H., Tong, D., Qin, W., Cheng, W., Liu, W., Fu, Q., Liu, B., Chai, F., Davis, S.J., Zhang, Q.,
283 He, K., 2020. Enhanced secondary pollution offset reduction of primary emissions during COVID-19 lockdown in China.
284 *National Science Review.*

285 Hutzell, W.T., Luecken, D.J., Appel, K.W., Carter, W.P.L., 2012. Interpreting predictions from the SAPRC07 mechanism based
286 on regional and continental simulations. *Atmos. Environ.* 46, 417-429.

287 Im, U., Markakis, K., Poupkou, A., Melas, D., Unal, A., Gerasopoulos, E., Daskalakis, N., Kindap, T., Kanakidou, M., 2011.
288 The impact of temperature changes on summer time ozone and its precursors in the Eastern Mediterranean. *Atmos Chem*
289 *Phys.* 11, 3847-3864.

290 Janssens-Maenhout, G., Crippa, M., Guizzardi, D., Dentener, F., Muntean, M., Pouliot, G., Keating, T., Zhang, Q., Kurokawa,
291 J., Wankmuller, R., van der Gon, H.D., Kuenen, J.J.P., Klimont, Z., Frost, G., Darras, S., Koffi, B., Li, M., 2015.
292 HTAP_v2.2: a mosaic of regional and global emission grid maps for 2008 and 2010 to study hemispheric transport of air
293 pollution. *Atmos Chem Phys.* 15, 11411-11432.

294 Lelieveld, J., Crutzen, P.J., 1990. Influences of Cloud Photochemical Processes on Tropospheric Ozone. *Nature.* 343, 227-233.

295 Li, K., Jacob, D.J., Liao, H., Shen, L., Zhang, Q., Bates, K.H., 2019a. Anthropogenic drivers of 2013-2017 trends in summer
296 surface ozone in China. *P Natl Acad Sci USA.* 116, 422-427.

297 Li, K., Jacob, D.J., Liao, H., Zhu, J., Shah, V., Shen, L., Bates, K.H., Zhang, Q., Zhai, S., 2019b. A two-pollutant strategy for

298 improving ozone and particulate air quality in China. *Nat Geosci.* 12, 906-910.

299 Li, M., Zhang, Q., Kurokawa, J., Woo, J.H., He, K.B., Lu, Z.F., Ohara, T., Song, Y., Streets, D.G., Carmichael, G.R., Cheng,
300 Y.F., Hong, C.P., Huo, H., Jiang, X.J., Kang, S.C., Liu, F., Su, H., Zheng, B., 2017. MIX: a mosaic Asian anthropogenic
301 emission inventory under the international collaboration framework of the MICS-Asia and HTAP. *Atmos Chem Phys.* 17,
302 935-963.

303 Li, R., Pei, S., Chen, B., Song, Y., Zhang, T., Yang, W., Shaman, J., 2020. Substantial undocumented infection facilitates the
304 rapid dissemination of novel coronavirus (SARS-CoV-2). *Science.* 368, 489-493.

305 Li, R., Wang, Z., Cui, L., Fu, H., Zhang, L., Kong, L., Chen, W., Chen, J., 2019c. Air pollution characteristics in China during
306 2015–2016: Spatiotemporal variations and key meteorological factors. *Sci. Total Environ.* 648, 902-915.

307 Lian, X., Huang, J., Huang, R., Liu, C., Wang, L., Zhang, T., 2020. Impact of city lockdown on the air quality of COVID-19-
308 hit of Wuhan city. *Sci. Total Environ.* 742, 140556.

309 Liu, F., Page, A., Strode, S.A., Yoshida, Y., Choi, S., Zheng, B., Lamsal, L.N., Li, C., Krotkov, N.A., Eskes, H., van der A, R.,
310 Veefkind, P., Levelt, P.F., Hauser, O.P., Joiner, J., 2020. Abrupt decline in tropospheric nitrogen dioxide over China after
311 the outbreak of COVID-19. *Science Advances.* 6, eabc2992.

312 Liu, Y., Wang, T., 2020a. Worsening urban ozone pollution in China from 2013 to 2017 – Part 1: The complex and varying
313 roles of meteorology. *Atmos. Chem. Phys.* 20, 6305-6321.

314 Liu, Y., Wang, T., 2020b. Worsening urban ozone pollution in China from 2013 to 2017 – Part 2: The effects of emission
315 changes and implications for multi-pollutant control. *Atmos. Chem. Phys.* 20, 6323-6337.

316 Lu, X., Hong, J.Y., Zhang, L., Cooper, O.R., Schultz, M.G., Xu, X.B., Wang, T., Gao, M., Zhao, Y.H., Zhang, Y.H., 2018.
317 Severe Surface Ozone Pollution in China: A Global Perspective. *Environ Sci Tech Let.* 5, 487-494.

318 Lu, X., Zhang, L., Chen, Y., Zhou, M., Zheng, B., Li, K., Liu, Y., Lin, J., Fu, T.M., Zhang, Q., 2019. Exploring 2016–2017
319 surface ozone pollution over China: source contributions and meteorological influences. *Atmos. Chem. Phys.* 19, 8339-
320 8361.

321 Ma, T., Duan, F.K., He, K.B., Qin, Y., Tong, D., Geng, G.N., Liu, X.Y., Li, H., Yang, S., Ye, S.Q., Xu, B.Y., Zhang, Q., Ma,

322 Y.L., 2019. Air pollution characteristics and their relationship with emissions and meteorology in the Yangtze River Delta
323 region during 2014-2016. *J. Environ. Sci.* 83, 8-20.

324 Miyazaki, K., Bowman, K., Sekiya, T., Jiang, Z., Chen, X., Eskes, H., Ru, M., Zhang, Y., Shindell, D., 2020. Air Quality
325 Response in China Linked to the 2019 Novel Coronavirus (COVID-19) Lockdown. *Geophys Res Lett.* 47,
326 e2020GL089252.

327 Murphy, B.N., Woody, M.C., Jimenez, J.L., Carlton, A.M.G., Hayes, P.L., Liu, S., Ng, N.L., Russell, L.M., Setyan, A., Xu, L.,
328 Young, J., Zaveri, R.A., Zhang, Q., Pye, H.O.T., 2017. Semivolatile POA and parameterized total combustion SOA in
329 CMAQv5.2: impacts on source strength and partitioning. *Atmos. Chem. Phys.* 17, 11107-11133.

330 Pye, H.O.T., Murphy, B.N., Xu, L., Ng, N.L., Carlton, A.G., Guo, H., Weber, R., Vasilakos, P., Appel, K.W., Budisulistiorini,
331 S.H., Surratt, J.D., Nenes, A., Hu, W., Jimenez, J.L., Isaacman-VanWertz, G., Misztal, P.K., Goldstein, A.H., 2017. On
332 the implications of aerosol liquid water and phase separation for organic aerosol mass. *Atmos. Chem. Phys.* 17, 343-369.

333 Roelofs, G.-J., Lelieveld, J., 1997. Model study of the influence of cross-tropopause O₃ transports on tropospheric O₃ levels.
334 *Tellus B: Chemical and Physical Meteorology.* 49, 38-55.

335 Seinfeld, J.H., Pandis, S.N., 2006. *Atmospheric Chemistry and Physics—from Air Pollution to Climate Change.* John Wiley &
336 Sons, New Jersey.

337 Shan, W., Yin, Y., Zhang, J., Ding, Y., 2008. Observational study of surface ozone at an urban site in East China. *Atmos Res.*
338 89, 252-261.

339 Sharma, S., Zhang, M., Anshika, Gao, J., Zhang, H., Kota, S.H., 2020. Effect of restricted emissions during COVID-19 on air
340 quality in India. *Sci. Total Environ.* 728, 138878.

341 Shi, X., Brasseur, G.P., 2020. The Response in Air Quality to the Reduction of Chinese Economic Activities During the
342 COVID-19 Outbreak. *Geophys Res Lett.* 47, e2020GL088070.

343 Sicard, P., De Marco, A., Agathokleous, E., Feng, Z., Xu, X., Paoletti, E., Rodriguez, J.J.D., Calatayud, V., 2020. Amplified
344 ozone pollution in cities during the COVID-19 lockdown. *Sci. Total Environ.* 735, 139542.

345 Siciliano, B., Dantas, G., da Silva, C.M., Arbilla, G., 2020. Increased ozone levels during the COVID-19 lockdown: Analysis

346 for the city of Rio de Janeiro, Brazil. *Sci. Total Environ.* 737, 139765.

347 Song, C.B., Wu, L., Xie, Y.C., He, J.J., Chen, X., Wang, T., Lin, Y.C., Jin, T.S., Wang, A.X., Liu, Y., Dai, Q.L., Liu, B.S., Wang,
348 Y.N., Mao, H.J., 2017. Air pollution in China: Status and spatiotemporal variations. *Environ. Pollut.* 227, 334-347.

349 Stadtler, S., Simpson, D., Schröder, S., Taraborrelli, D., Bott, A., Schultz, M., 2018. Ozone impacts of gas-aerosol uptake in
350 global chemistry transport models. *Atmos. Chem. Phys.* 18, 3147-3171.

351 Steiner, A.L., Davis, A.J., Sillman, S., Owen, R.C., Michalak, A.M., Fiore, A.M., 2010. Observed suppression of ozone
352 formation at extremely high temperatures due to chemical and biophysical feedbacks. *Proceedings of the National
353 Academy of Sciences.* 107, 19685-19690.

354 Sun, Y., Wang, Y., Zhang, C., 2009. Vertical observations and analysis of PM_{2.5}, O₃, and NO_x at Beijing and Tianjin from towers
355 during summer and Autumn 2006. *Advances in Atmospheric Sciences.* 27, 123.

356 Tonnesen, G.S., Dennis, R.L., 2000. Analysis of radical propagation efficiency to assess ozone sensitivity to hydrocarbons and
357 NO_x : 1. Local indicators of instantaneous odd oxygen production sensitivity. *J. Geophys. Res.-Atmos.* 105, 9213-9225.

358 Wang, P., Chen, K., Zhu, S., Wang, P., Zhang, H., 2020a. Severe air pollution events not avoided by reduced anthropogenic
359 activities during COVID-19 outbreak. *Resources, Conservation and Recycling.* 158, 104814.

360 Wang, S., Zhao, M., Xing, J., Wu, Y., Zhou, Y., Lei, Y., He, K., Fu, L., Hao, J., 2010. Quantifying the Air Pollutants Emission
361 Reduction during the 2008 Olympic Games in Beijing. *Environ Sci Technol.* 44, 2490-2496.

362 Wang, T., Xue, L.K., Brimblecombe, P., Lam, Y.F., Li, L., Zhang, L., 2017a. Ozone pollution in China: A review of
363 concentrations, meteorological influences, chemical precursors, and effects. *Sci. Total Environ.* 575, 1582-1596.

364 Wang, Y., Yuan, Y., Wang, Q., Liu, C., Zhi, Q., Cao, J., 2020b. Changes in air quality related to the control of coronavirus in
365 China: Implications for traffic and industrial emissions. *Sci. Total Environ.* 731, 139133.

366 Wang, Z., Li, Y., Chen, T., Li, L., Liu, B., Zhang, D., Sun, F., Wei, Q., Jiang, L., Pan, L., 2015. Changes in atmospheric
367 composition during the 2014 APEC conference in Beijing. 120, 12695-12707.

368 Wang, Z.S., Li, Y.T., Zhang, D.W., Chen, T., Wei, Q., Sun, T.H., Wang, B.Y., Pan, J.X., Cui, J.X., Pi, S., 2017b. Analysis on
369 air quality in Beijing during the military parade period in 2015. *China Environ. Sci.* 37, 1628-1636.

370 WHO, 2020. Coronavirus Disease (COVID-2019) Situation Reports. World Health Organization

371 Wu, K., Kang, P., Tie, X., Gu, S., Zhang, X., Wen, X., Kong, L., Wang, S., Chen, Y., Pan, W., Wang, Z., 2019. Evolution and
372 Assessment of the Atmospheric Composition in Hangzhou and its Surrounding Areas during the G20 Summit. *Aerosol*
373 *Air Qual Res.* 9, 2757-2769.

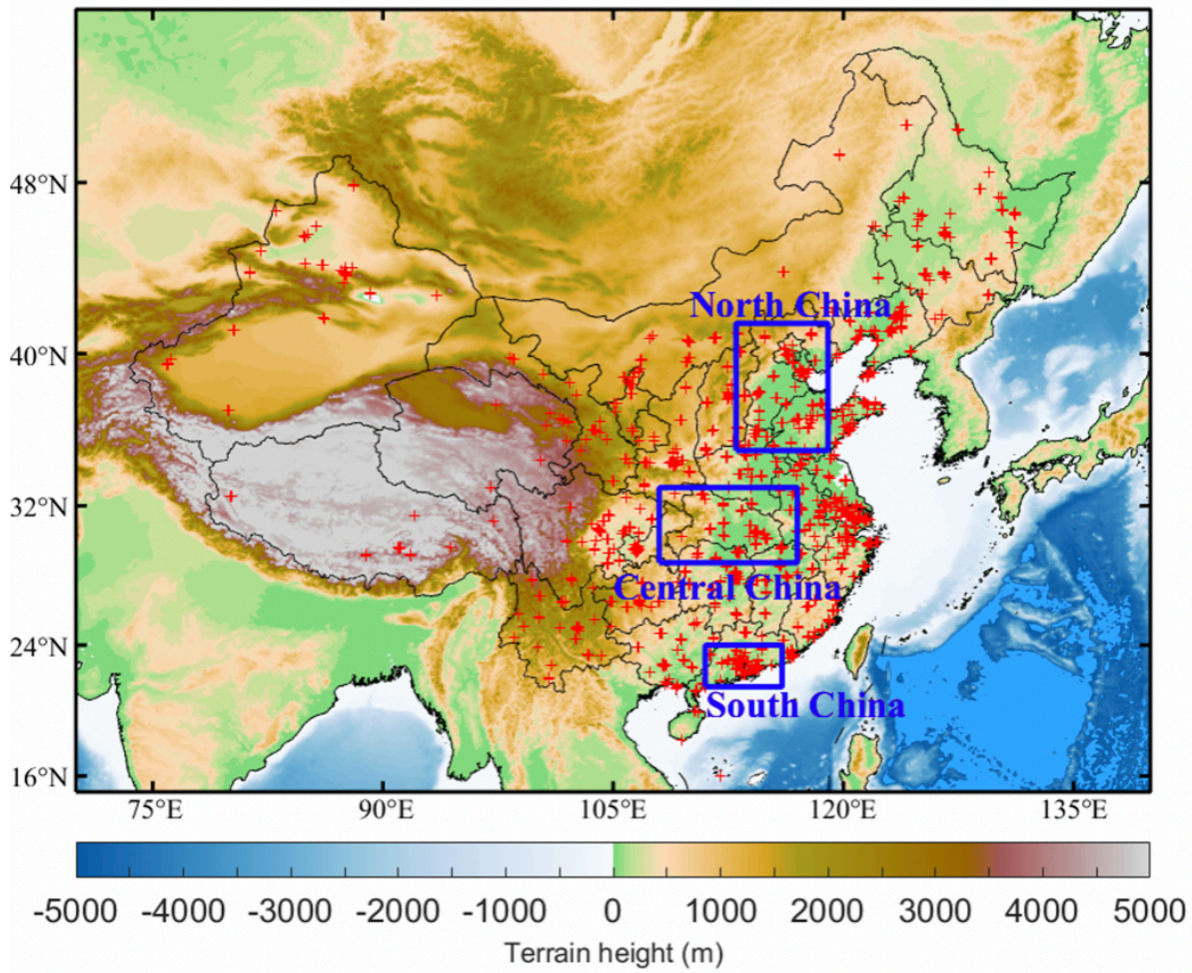
374 Wu, K., Yang, X., Chen, D., Gu, S., Lu, Y., Jiang, Q., Wang, K., Ou, Y., Qian, Y., Shao, P., Lu, S., 2020. Estimation of biogenic
375 VOC emissions and their corresponding impact on ozone and secondary organic aerosol formation in China. *Atmos Res.*
376 231, 104656.

377 Zhang, R., Zhang, Y., Lin, H., Feng, X., Fu, T.-M., Wang, Y., 2020. NO_x Emission Reduction and Recovery during COVID-
378 19 in East China. *Atmosphere* 11, 433.

379 Zheng, B., Tong, D., Li, M., Liu, F., Hong, C., Geng, G., Li, H., Li, X., Peng, L., Qi, J., Yan, L., Zhang, Y., Zhao, H., Zheng,
380 Y., He, K., Zhang, Q., 2018. Trends in China's anthropogenic emissions since 2010 as the consequence of clean air actions.
381 *Atmos. Chem. Phys.* 18, 14095-14111.

382 Zhu, S., Poetscher, J., Shen, J., Wang, S., Wang, P., Zhang, H.J.a.p.a., 2020. The seesaw impacts between reduced emissions
383 and enhanced AOC on O₃ during the COVID-19.

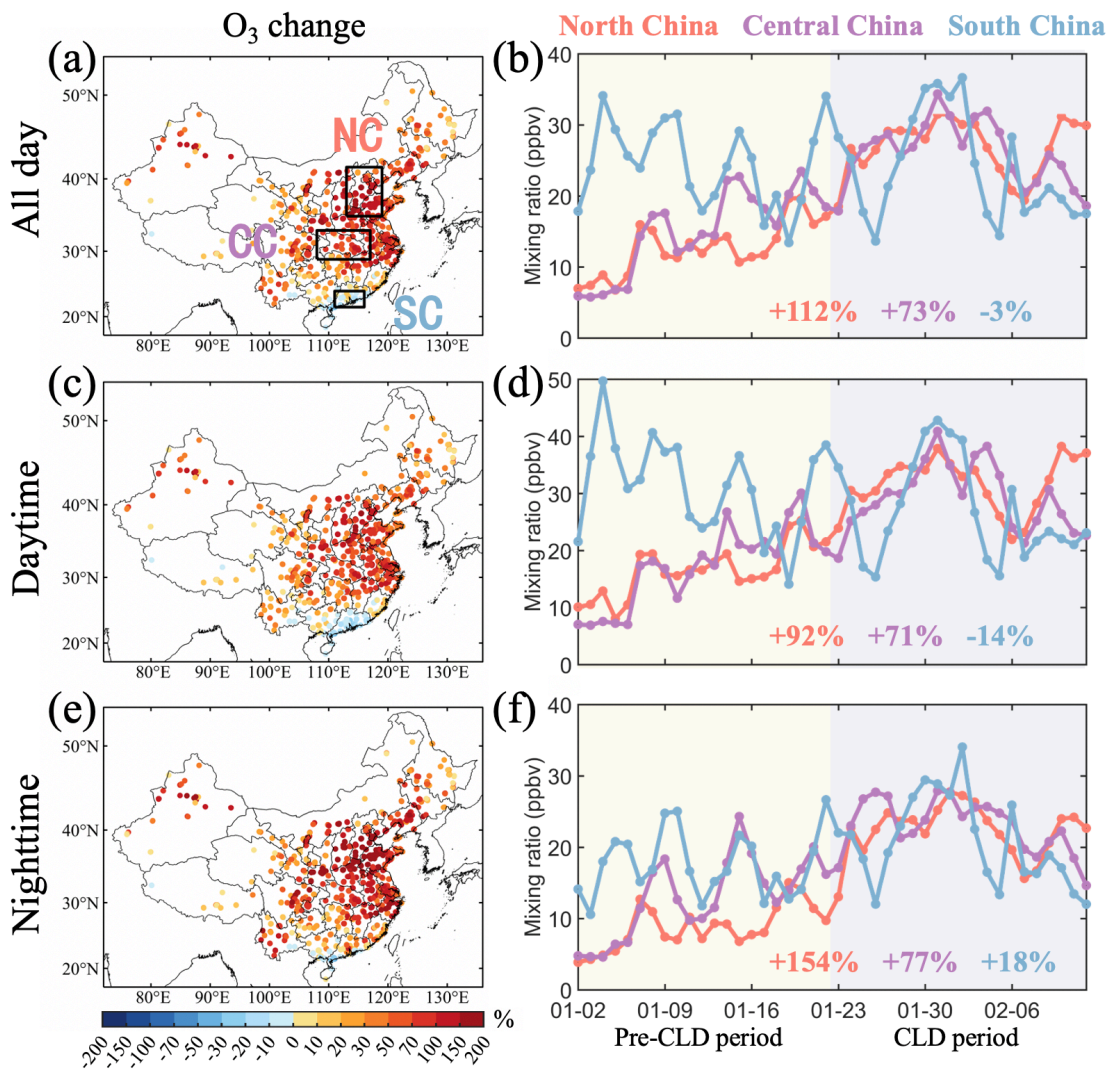
384



385

386 Figure 1: Location of 1643 environmental monitoring stations (red “+” symbols) operated by the Ministry of Ecology and Environmental
387 Protection of China. The blue boxes denote the regions of north China, central China, and south China designated for further analysis.

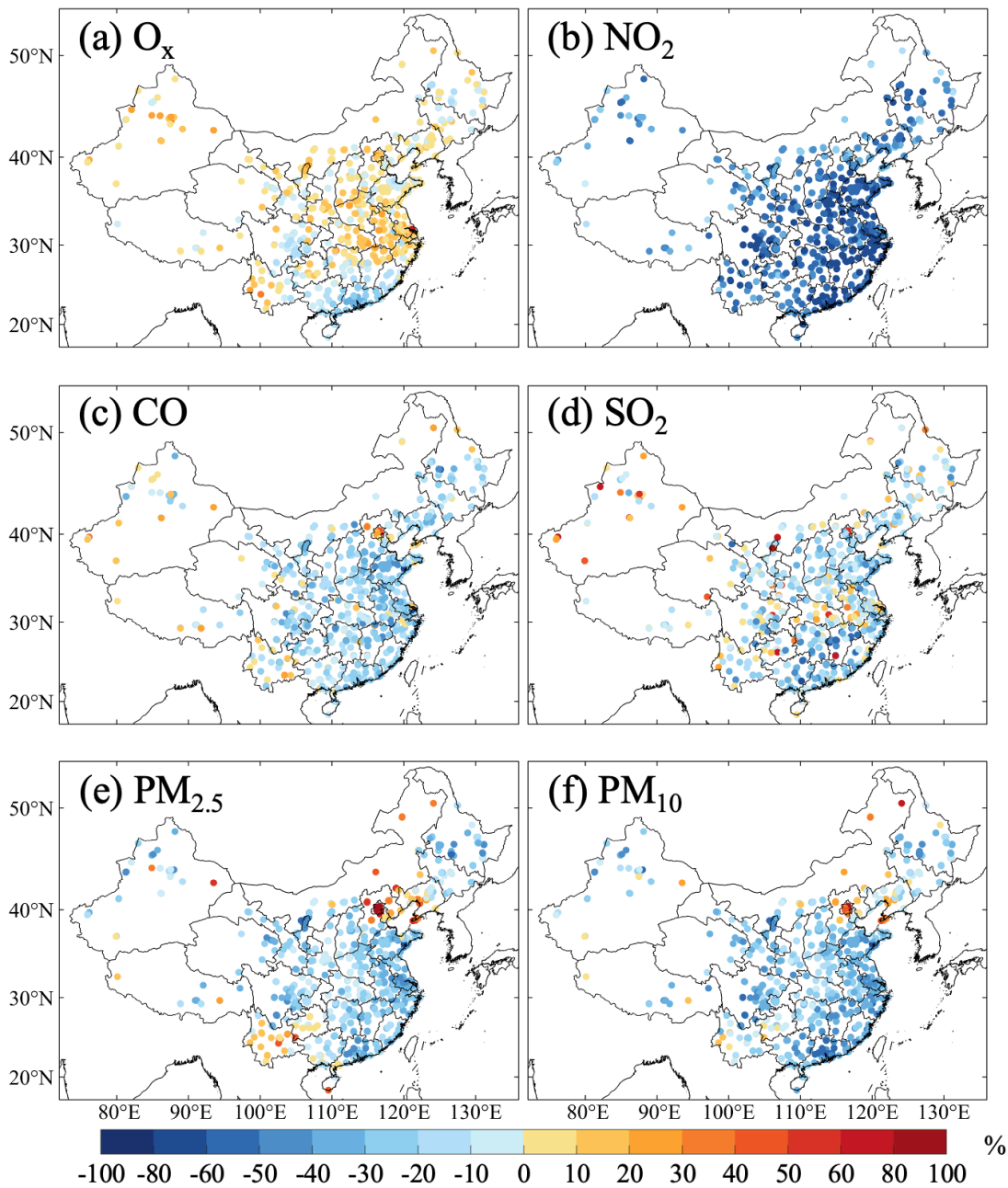
388



389

390 Figure 2: Observed changes in O₃ mixing ratios across mainland China before and during the COVID-19 lockdown period. (a, c, e) The
 391 spatial distribution of O₃ changes for all-day average, daytime average, and nighttime average during the CLD period compared with the
 392 pre-CLD period. The black boxes in (a) show the locations of north China (NC, 184 sites), central China (CC, 108 sites), and south China
 393 (SC, 77 sites). (b) The variations of all-day average O₃ mixing ratios during the study period for the NC, CC, and SC regions. (d) The same
 394 with (b) but for daytime average O₃. (f) The same with (b) but for nighttime average O₃.

395



396

397

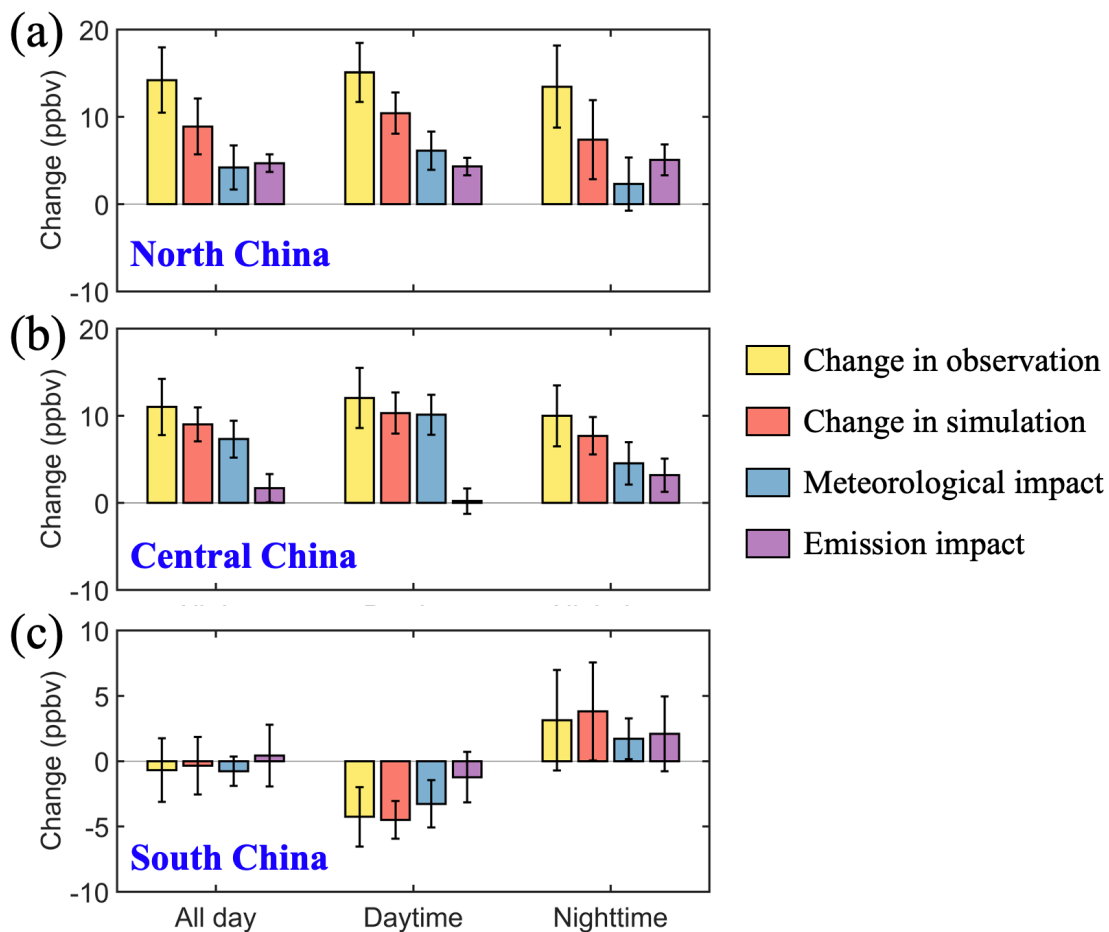
Figure 3: Percentage change of (a) observed daytime average O_x (NO_2+O_3), whole-day average (b) NO_2 , (c) CO, (d) SO_2 , (e) $PM_{2.5}$, and (f)

398

PM_{10} concentrations during the CLD period relative to the pre-CLD period.

399

400



401

402

403

404

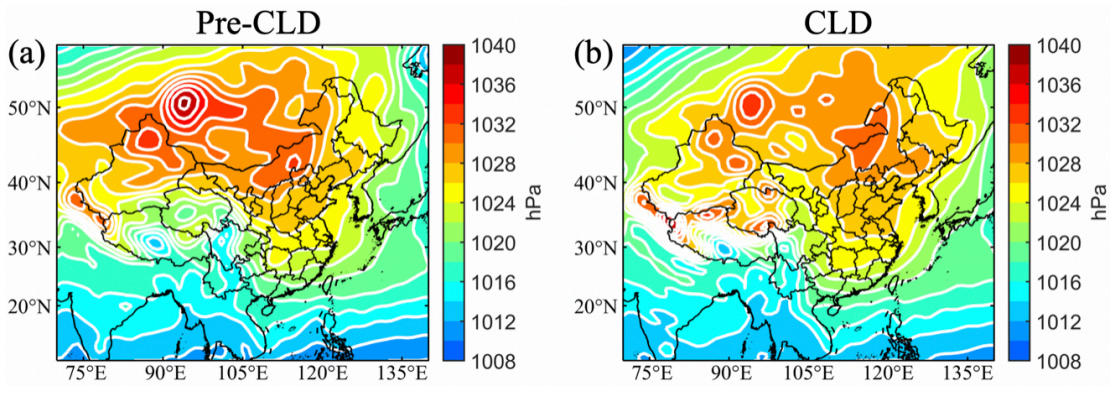
405

406

407

408

Figure 4: Changes in O₃ mixing ratios during the COVID-19 lockdown period and contributions from meteorological changes and emission reductions for three typical regions. (a) Observed and simulated changes in O₃ mixing ratios and the contributions from meteorological changes and emission reductions during the CLD period compared with the pre-CLD period in north China (NC). The O₃ changes for the all-day average, daytime average, and nighttime average are presented. (b) The same with (a) but for central China (CC). (c) The same with (a) but for south China (SC). The locations of these three regions are shown in Fig. 1. Note that the error bars mark the standard deviations within the region.



409

410

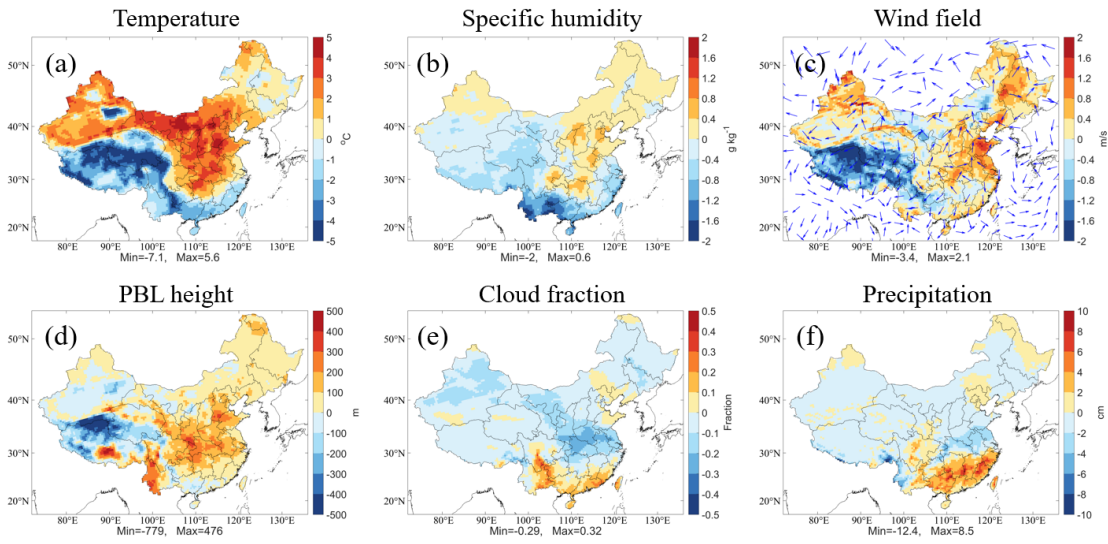
Figure 5: Averaged sea-level pressure during the pre-CLD and CLD periods. Data are from the National Center for Environmental Prediction

411

(NCEP) FNL Operational Model Global Tropospheric Analyses dataset.

412

413



414

415

Figure 6: Model simulated changes in daytime temperature at 2 m height, specific humidity at 2 m height, wind field at 10 m height, planetary

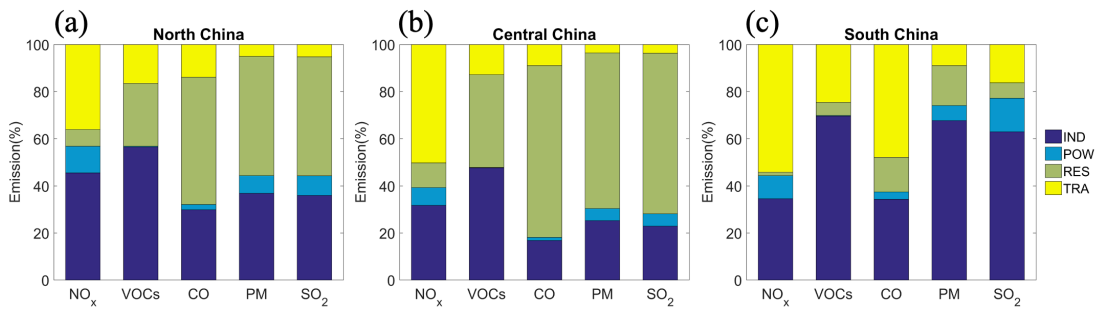
416

boundary layer (PBL) height, cloud fraction, and precipitation during CLD period relative to pre-CLD period. In panel (c), the shaded color

417

and vector represent the wind speed and wind direction, respectively.

418



419

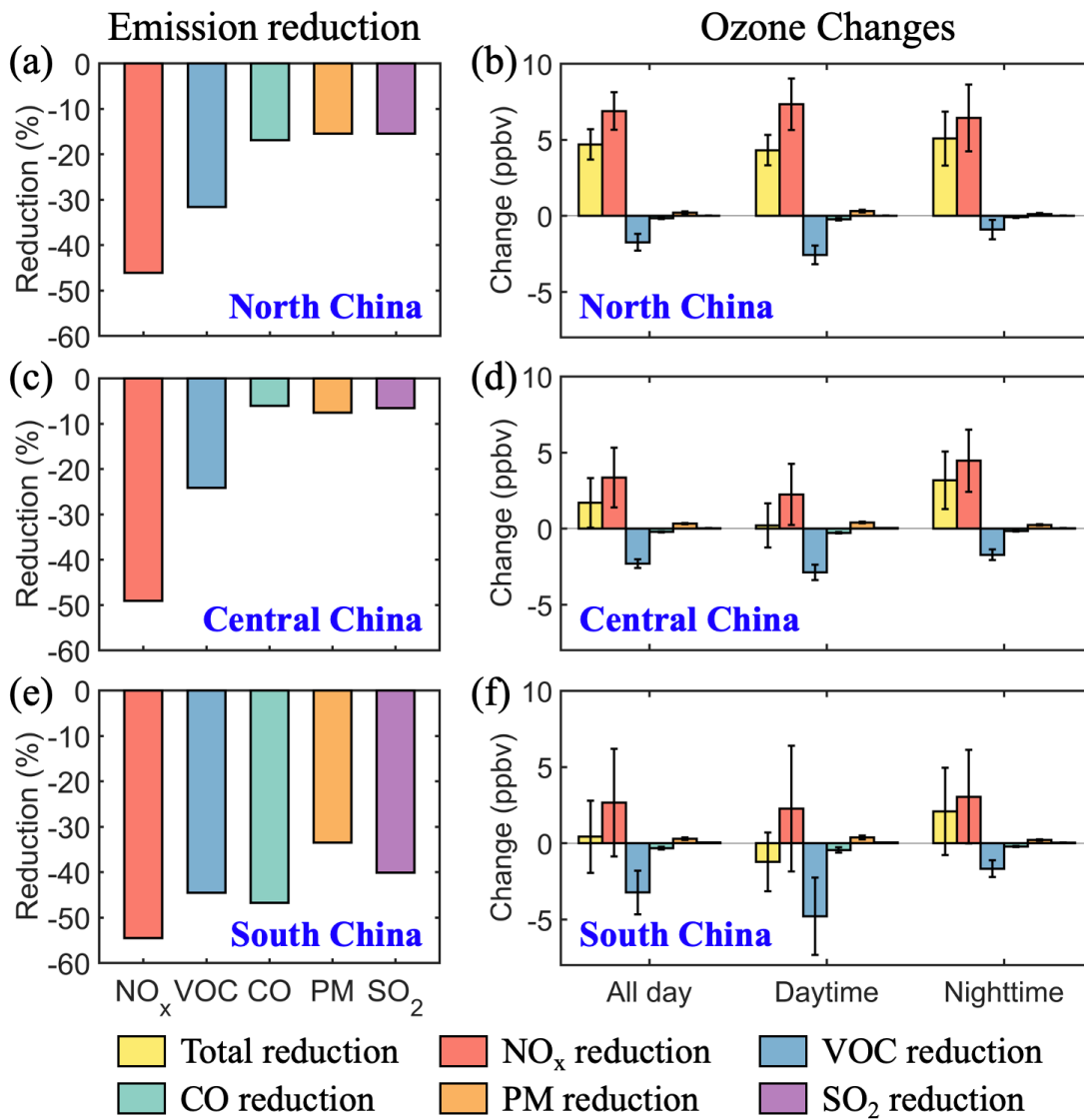
420

421

422

423

Figure 7: Percentage contribution to NO_x, VOCs, CO, PM, and SO₂ emissions from industrial (IND), power plant (POW), residential (RES), and transportation (TRA) sectors in (a) north China, (b) central China, and (c) south China. Emission data are from 2017 MEIC (<http://meicmodel.org>) with estimated scaling factors from 2017 to 2020.



424

425

426

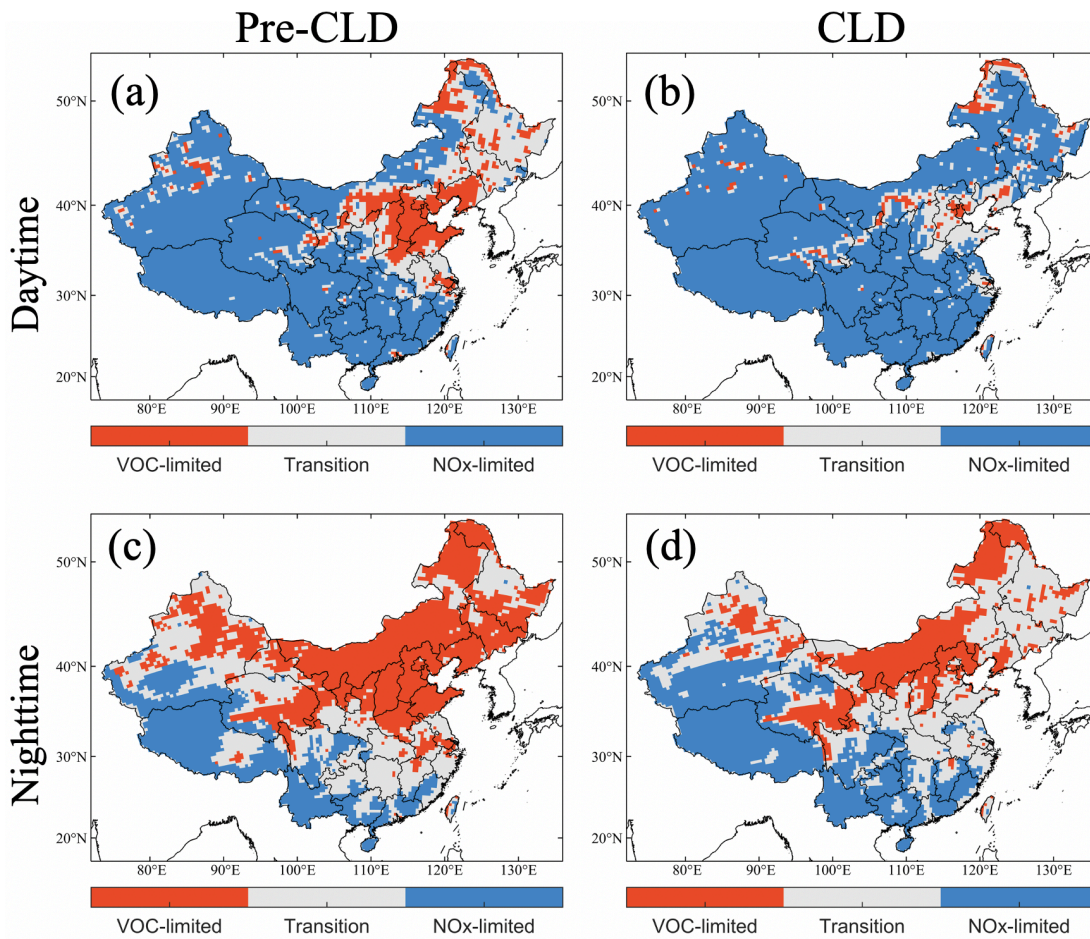
427

428

429

430

Figure 8: The estimated reductions of multi-pollutant emissions due to the COVID-19 lockdown and their impacts on the O₃ changes for three regions. (a, c, e) The estimated reductions of NO_x, VOC, CO, PM, and SO₂ emissions during the CLD period compared with the pre-CLD period for north China, central China, and south China. (b, d, f) The impacts of different pollutant emission reductions due to the lockdown on O₃ changes for the three regions. The O₃ changes for all-day average, daytime average, and nighttime average are presented. The error bars are the standard deviations.



431

432

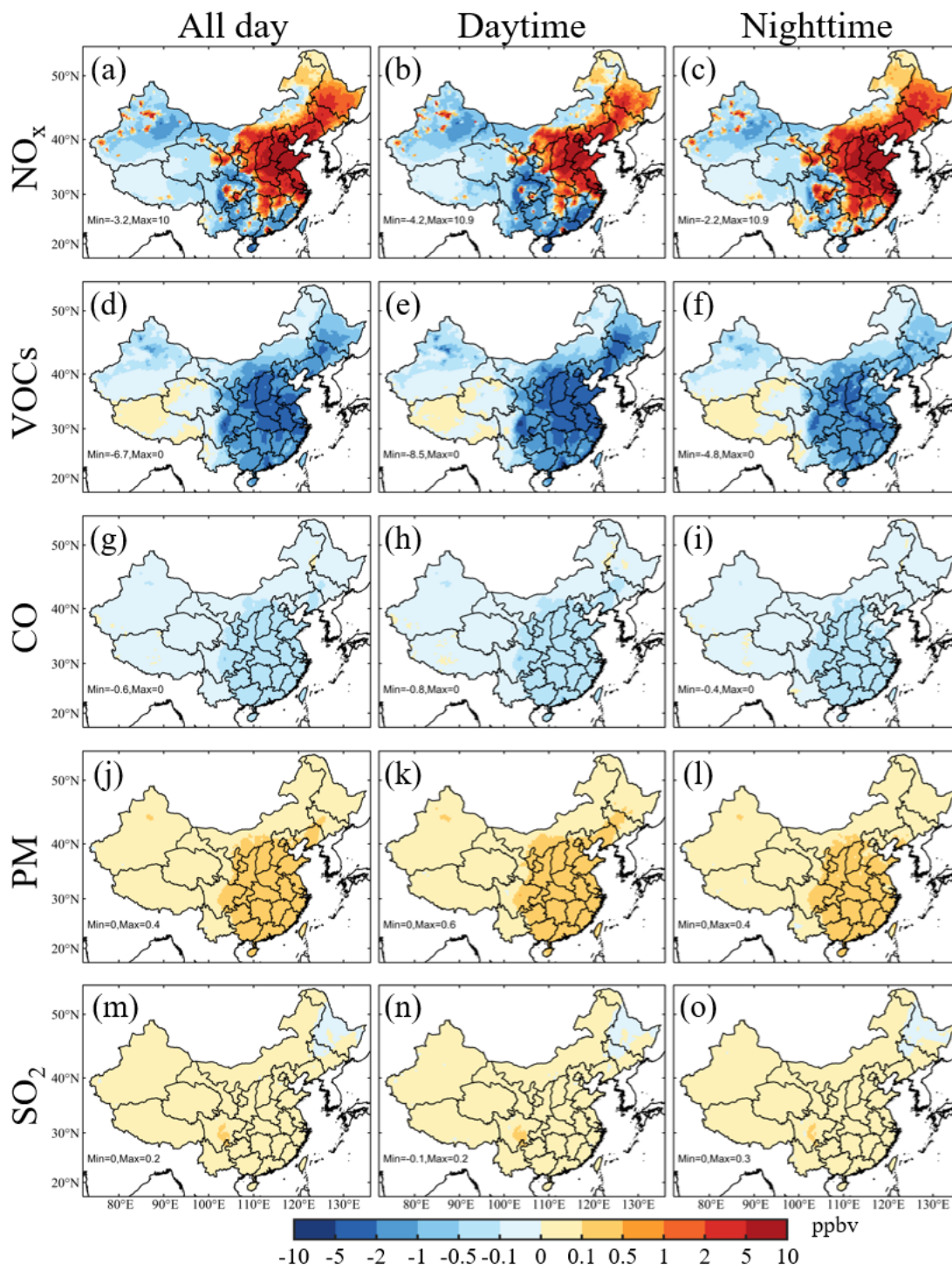
433

434

435

436

Figure 9: Ozone formation regime in the daytime and nighttime before and during the lockdown periods estimated by the ratio of the production rates of hydrogen peroxide to nitric acid ($P_{H_2O_2}/P_{HNO_3}$). VOC-limited region: $P_{H_2O_2}/P_{HNO_3} < 0.06$; NO_x -limited region: $P_{H_2O_2}/P_{HNO_3} \geq 0.2$, Transition zone: $0.06 \leq P_{H_2O_2}/P_{HNO_3} < 0.2$. The production rates of H_2O_2 and HNO_3 were calculated by the integrated reaction rate (IRR) diagnose tool in the CMAQ model.

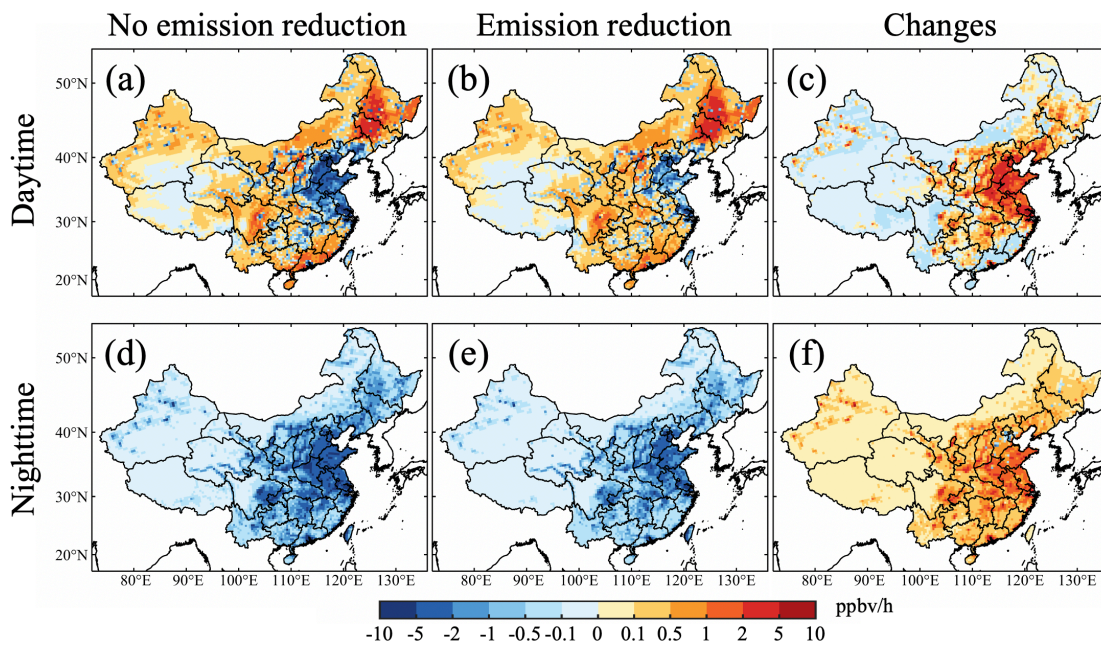


437

438 Figure 10: Model simulated changes in O₃ mixing ratios for all-day average, daytime average, and nighttime average due to the reductions

439 of NO_x, VOC, CO, PM, and SO₂ emissions during the CLD period compared with the pre-CLD period.

440



441

442 Figure 11: O₃ chemical production rates before and after the anthropogenic emission reductions and the changes during the COVID-19

443 lockdown period. The chemical production rates were calculated by the process analysis method in the CMAQ model.

444